Site exploration for anchoring of wave energy converters

Tuyen Ngoc Tran[1,2] and *T. Matthew* Evans[1#]

[1]*Oregon State University, School of Civil and Construction Engineering, Corvallis, OR USA 97331*
[2]*Hatinh University, Hatinh, Vietnam*
[#]*Corresponding author: matt.evans@oregonstate.edu*

ABSTRACT

Wave energy converters (WECs), a form of marine hydrokinetic (MHK) energy device, transform the mechanical energy of water waves into electricity. They are typically held on station using anchoring systems embedded into the seafloor sediments (as opposed to, e.g., concrete gravity anchors). The design of WEC anchors is particularly challenging for two primary reasons: (1) WECs are often deployed in previously undeveloped areas of the ocean, so the engineering properties of the seabed are largely unknown; and (2) the economic margins on wave energy are quite thin, so heavily overdesigned anchor systems in response to data sparsity are not feasible. This paper describes the planning, execution, and outcomes from a dedicated in-situ testing campaign informed only by limited geophysical data a priori. A series of 22 cone penetration tests (CPTs) were performed at a 7-km^2 site approximately 11 km off the United States' west coast. Water depth was up to approximately 75 m and the target depth for the cone soundings was 10.5 m below the seafloor. Measurements indicated that much of the site subsurface consisted of dense sand and gravel, though tests identified an overlying softer layer in some parts of the site. A summary of lessons learned and recommendations for future explorations at similarly unexplored sites are provided.

Keywords: soil classification, cone penetration test, wave energy converters, offshore testing

1. Site Overview

The PacWave South Test Site (STS, Fig. 1) is a pre-permitted, grid-connected, wave energy test facility located approximately 11.1 km (6 nmi) off the coast of Newport Oregon, on the United States' west coast (N.B., navigation measurements in nautical miles are exact throughout, with SI measurements provided for reference; 1 nmi ≙ 1852 m). It has been developed in partnership with the US Department of Energy, the State of Oregon, Oregon State University (OSU), and local stakeholders. The STS comprises an area of 6.9 km^2 (2 nmi^2) and consists of four berths, 1.7 km^2 (0.5 nmi^2) each. The STS will be grid-connected and is pre-permitted for the majority of wave energy device types. Grid connection is facilitated through four horizontal directionally drilled (HDD) bores, each with a length of over 1.6 km and up to 37 m below the seafloor. Shallow buried cable from the seafloor daylights of the HDD bores to the STS will allow for developers of wave energy converters (WECs) to simply "plug in" their devices upon deployment.

Site characterization is critical for optimizing WEC anchor design, whether in the initial stages to evaluate project viability or in the final stages before deployment. To that end, in support of the development of the PacWave STS, a field exploration program was undertaken in September 2023. The program consisted of advancement of 22 cone penetration tests (CPTs) across the STS (Fig. 2), each with a target depth of 10.5 m below the seafloor in 65 m-75 m of water. In-water work was staged off the 80-m *Seacor Lee* using an A.P. van den Berg ROSON 100 deployed by ConeTec with support from R.T. Casey, the PacWave cabling contractor.

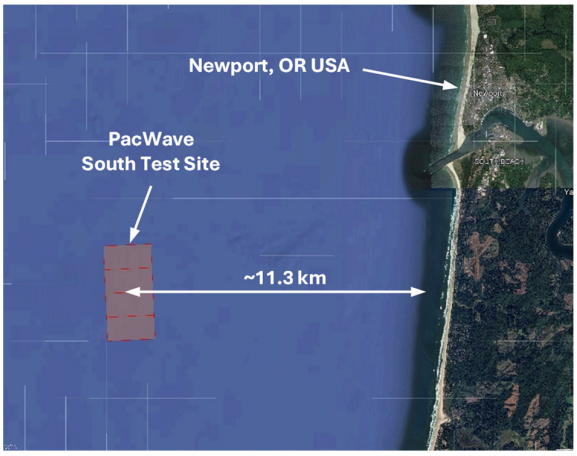

Figure 1. Location of the PacWave STS.

Reduction of CPT data collected with high overburden hydrostatic stresses can prove challenging, particularly at shallow depths, because the total stress field is quite different than that used to define common cone parameters or in development of correlations to engineering properties. It is possible, of course, to "zero out" stress by subtracting hydrostatic pressure at the sea floor, but this isn't strictly correct, either, as it fails to correctly predict the total stress effect accounted for in some relationships.In this paper we present results from select CPT soundings at the PacWave STS. We briefly

explore the implications of a high total stress field in analyzing the data and soil profile variability across the site is discussed qualitatively.

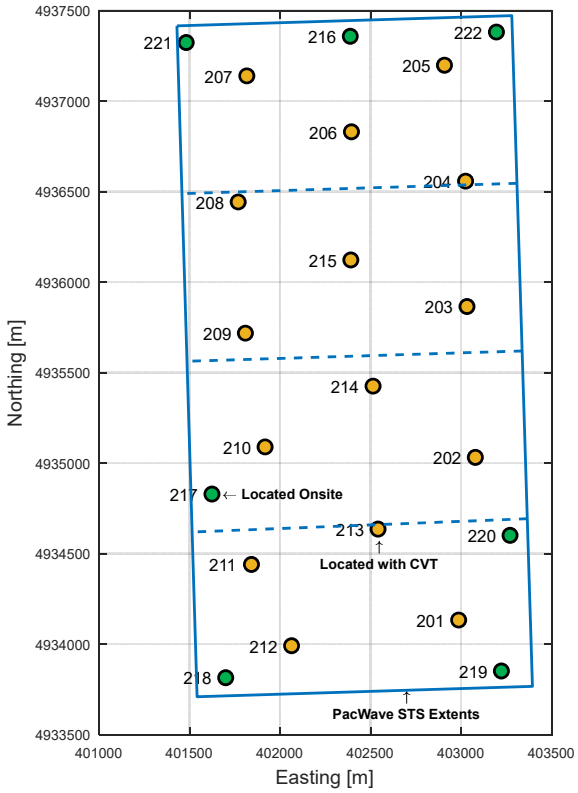

Figure 2. CPT locations at the PacWave STS.

2. Collection of CPT Data

2.1. Specifying Sounding Locations

We planned our in-water work with the expectation of performing a total of 20 CPTs across the site. Because we did not have appreciable subsurface data *a priori*, we decided to preselect 12 locations and then use the results from those soundings to inform selection of the final eight locations. The first 12 locations were initially planned on a regular grid within the STS bounds (solid lines in Fig. 2) such that each of the four berths (delineated by dashed lines in Fig. 2) received approximately equal coverage. However, there was concern that these locations would not provide sufficient coverage near the site boundaries, so ultimately, we elected to employ a different approach to select test locations: maximizing the disorder of the CPT spacing.

Entropy was first suggested as a means of characterizing the information content of a digital communication (or other Markov process) by Shannon (1948), who defined it as:

$$H \propto \sum_{i=1}^{n} p_i \log_2 p_i \qquad (1)$$

where the p_i are the individual probabilities of n independent events and the base-2 logarithm is used for application to binary signals. Jaynes (1957a; b) drew parallels to statistical mechanics, and the concept of maximum entropy as a measure of optimal state was subsequently adopted in a variety of applications (e.g., Brown 1978, 1980; Jowitt 1979; Krieger 1970; Morgenstern 1963). In application to the orientation of geologic materials, Shi et al. (1998) suggested that a more appropriate base to the logarithm would be n:

$$H_m = -\sum_{i=1}^{n} P_i \log_n P_i \qquad (2)$$

where P_i is the probability that an object will exist in the i^{th} state and switching to base-n logarithms results in $H_m \in [0,1]$ where $H_m = 0$ corresponds to perfect order (all objects in a single bin) and $H_m = 1$ corresponds to perfect disorder (all bins having the same number of objects). This modified definition of Shannon entropy has been previously employed to effectively characterize disorder in both physical and numerical assemblies of particles (Evans and Brown 2014; Evans and Frost 2010).

In an attempt to maximize the entropy of CPT locations, we used a centroidal Voronoi tessellation (CVT; e.g., Du et al. 1999; Hateley et al. 2015) to subdivide the PacWave STS. In CVT, the generating point of each Voronoi cell is also its centroid. We randomly select 15 points within the extents of the STS and then perform Voronoi relaxation (Lloyd's algorithm; Lloyd 1982) to asymptotically approach the optimal spacing. We then compute the distance between each sounding and every other sounding and determine the entropy of the histogram of the computed distances. An example CVT diagram for the PacWave STS and its associated distance histogram are shown in Fig. 3. We note that the entropy value ($H_m = 0.9237$) is quite close to unity.

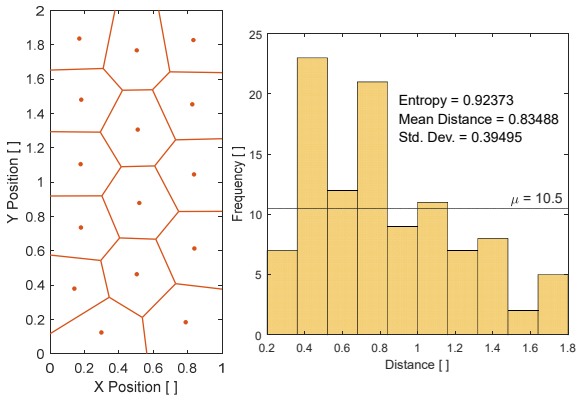

Figure 3. A CVT of the PacWave STS and the histogram of distances between all centroids (i.e., CPT locations).

The orange data points in Fig. 2 are the 15 pre-selectd CPT locations determined through CVT and correspond to the points identified in Fig. 3: i.e., the arrangement shown empirically to have the maximum disorder. Results from these 15 soundings were analyzed in real time to develop a qualitative sense of subsurface properties. Results were observed to vary more along the north-south axis of the site than the east-west axis. An additional seven soundings were selected (shown in green in Fig. 2) to provide finer detail about the subsurface property variability at the site, as discussed subsequently.

2.2. Cone Penetration Testing

After appreciable delays due to sea state, testing was ultimately performed over a period of 33 consecutive hours, resulting in the 22 CPT soundings discussed previously. All but two soundings (CPT-202 and CPT-204) reached the target depth of approximately 10.5 m. Tip resistance (q_c, subsequently corrected to $q_t = q_c + (1-a)u_2; a = 0.75$), sleeve friction ($f_s$), and pore water pressure (u_2) were measured every 2 cm during each push. Preliminary data from the first 15 soundings indicated that there was a softer layer of material near the surface underlain by stiff layer that generated significant negative excess pore water pressures during cone advancement. The thickness of the overlying softer layer was up to 6 m at the southern end of the site transitioning to less than 1 m at the northern site boundary. As such, we elected to perform several additional pushes near the southern end of the site to better delineate the soft layer.

3. Measured Results

Figs. 4 and 5 present results from typical soundings at the southern (CPT-212) and northern (CPT-207) areas of the site, respectively. Results from CPT-212 show relatively low tip resistance and sleeve friction to a depth of 5-6 m and high positive excess pore water pressure down to a depth of slightly more than 4 m, all implying a thick layer of softer, fine-grained material. Conversely, there is not a significant thickness of softer sediments readily observable in CPT-207.

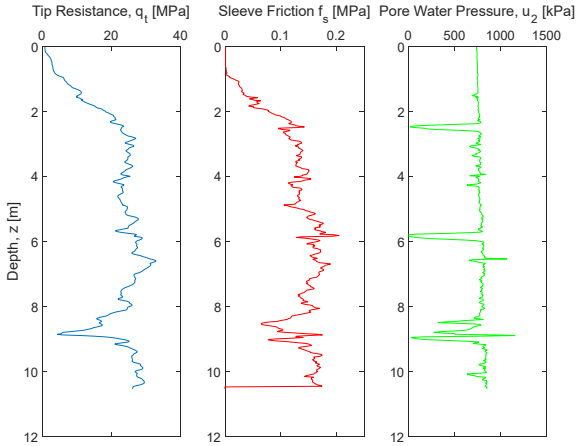

Figure 4. Sounding CPT-207 at the PacWave STS.

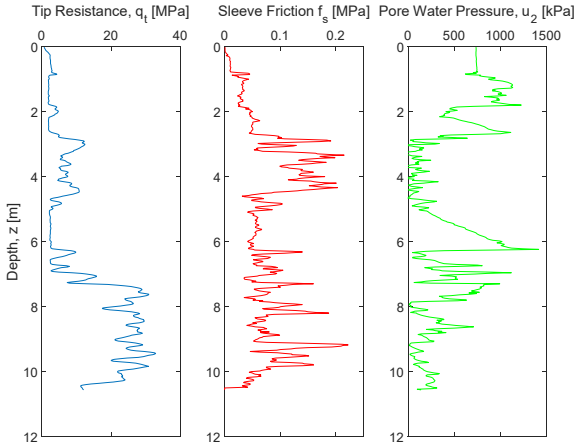

Figure 5. Sounding CPT-212 at the PacWave STS.

4. Synthesis and discussion

Piezocone data is commonly interpreted through the lens of normalized soil behavior type (SBT_n), which can have several different definitions. Three common SBT_n charts are presented in Fig. 6 with data from CPT-207 and CPT-212 (see Fig. 2 for locations). All three figures incorporate cone tip resistance through the normalized tip resistance with a variable stress exponent:

$$Q_{tn} = \frac{q_n}{p_a}\left(\frac{p_a}{\sigma'_{v0}}\right)^n \tag{3}$$

$$n = 0.381 I_c + 0.05\left(\frac{\sigma'_{v0}}{p_a}\right) - 0.15 \leq 1 \tag{4}$$

where $q_n = q_t - \sigma_{v0}$ is net cone tip resistance; σ_{v0} and σ'_{v0} are total and effective in-situ stresses, respectively; p_a is standard atmospheric pressure; and I_c is the SBT_n index. Each of the three figures use a different quantity on the ordinate of the plot, however. From left to right, these are normalized friction ratio (F), normalized excess pore pressure ($\Delta u_2/\sigma'_{v0}$), and normalized small-strain shear modulus (I_G):

$$F = \frac{f_s}{q_n} \cdot 100\% \tag{5}$$

$$\Delta u_2 = u_2 - u_0 \tag{6}$$

where u_0 is hydrostatic pore water pressure and G_0 is small-strain shear modulus, which is computed using

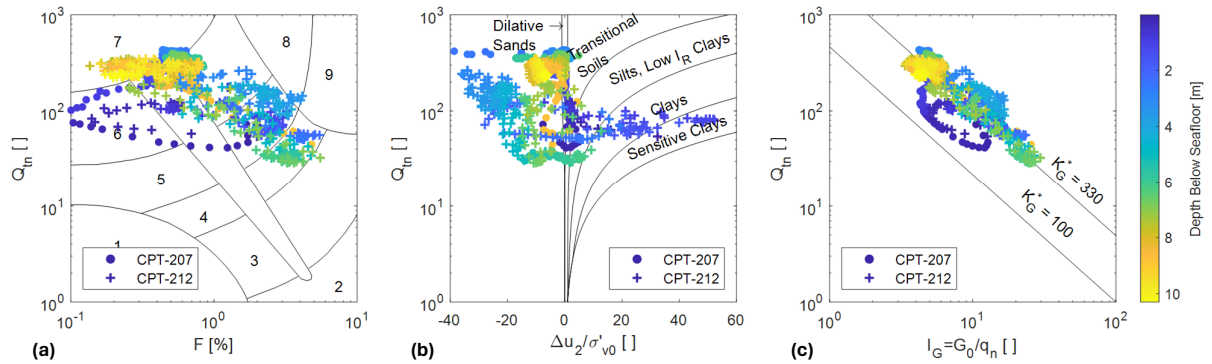

Figure 6. Three soil behavioral classifications for two of the soundings at PacWave South, from L to R: Robertson (2009); Schneider et al. (2008) as modified by Robertson (2009); and Schneider and Moss (2011).

densities and shear wave velocities correlated from CPT measurements.

Data in Fig. 6(a) shows that soils at shallower depths generally plot in SBT_n zones 4 (silt mixtures – clayey silt to silty clay) and 5 (sand mixtures – silty sand to sandy silt), particularly in CPT-212. Moving deeper into the profiles, measurements move towards Zones 6 (sands – clean sand to silty sand) and 7 (gravelly sand to dense sand), with very tight clustering of data indicating relatively little variability in soil behavior. Figure 6(b) highlights the softer (low Q_{tn}) materials in CPT-212 moving from positive to negative excess pore water pressures as depth increases, with the deepest material ultimately lying in the dilative sand range. Data for CPT-207 generally in or near the dilatant sand region with clustering similar to that observed in Fig. 6(a). The data in Fig. 6(c) are seen to largely lie along the $K_G^* = 330$ line where K_G^* is the modified normalized small strain rigidity index (Robertson 2016), a measure of the relative importance of stiffness and strength in the behavior of a given soil. Schneider and Moss (2011) adopted an unmodified $K_G \geq 330$ as an indicator of aged, calcareous, or cemented sands (N.B., K_G is calculated using q_t while K_G^* uses q_n). Robertson (2016) notes, however, that using q_n to define K_G^* allows for its usage to be expanded to fine-grained soils as well and suggests that $K_G^* \geq 330$ indicates a soil having significant microstructure, implying that these materials may not be readily amenable to characterization with some existing empirical correlations.

5. Implications for Anchor Design

The types of anchors that will be deployed at PWS are not yet known. However, two anchor types that are widely used for loading scenarios similar to those anticipated for WECs in an energetic wave environment are plate anchors and torpedo anchors. We can use some of the cone data interpretations to make inferences about anchor design. Figure 7 presents SBT_n plots for a north-south transect at PWS. Data at 0.5-m depths (for clarity) from six CPT soundings is presented. The observed trends are similar to those seen in Fig. 6: soils at shallower depths are softer and finer-grained than those at depth; there is tight clustering of data, indicating consistency in soil properties; and modified normalized small-strain rigidity indices indicate that many of the soils have structure, especially the deeper deposits.

The pullout capacity of plate anchors is a function of surrounding soil strength and embedment ratio, $\lambda = H_0/B$, where H_0 is embedment depth and B is anchor width. Capacity is typically characterized in terms of breakout factor, N_γ, defined as the ultimate pullout capacity normalized by the weight of soil above the anchor. In a comparison of discrete element method (DEM) simulations to several closed-form limiting equilibrium expressions for breakout factor, Evans and Zhang (2019) show that for a friction angle of $\phi' = 24°$, breakout factor is expected to vary from 3-15 for an embedment ratio of $\lambda = 6$. We select this embedment ratio for further discussion because the thickness of the overlying softer layer in some areas of PWS is up to 6 m. We expect anchor installation to be more straightforward through the softer material than into the dense sands and gravels underneath: a square plate anchor with a side length of 1 m installed at the approximate maximum depth of the softer layer would result in $\lambda = 6$.

The holding capacity of a torpedo anchor is a strong function of its embedment depth, which in turn depends on anchor geometry, impact velocity, and the properties of the seabed. The following expression has been suggested (Hossain et al. 2015; O'Loughlin et al. 2013) for calculation of the tip embedment (z_e) of a torpedo anchor:

$$\frac{z_e}{d_{eff}} \approx \left(\frac{E_{tot}}{k \cdot d_{eff}^4}\right)^{\frac{1}{p}} \tag{7}$$

$$E_{tot} = \frac{1}{2} m v_i^2 + m' g z_e \tag{8}$$

where d_{eff} is effective anchor diameter (i.e., accounting for the presence of flukes); k is the undrained shear strength gradient in the seabed ($\propto$ kPa/m); m is anchor mass; m' is effective anchor mass (mass submerged in soil); v_i is impact velocity, $g = 9.81\ \mathrm{m/s^2}$; and p is an empirically-determined exponent (e.g., $p = 3$ for overconsolidated clay and $p = 3.24$ for calcareous silt). Ehlers et al. (2004) reports that anchor penetration into sands is similar to that in overconsolidated clay, implying that $p = 3$ may also be appropriate for sands. This is consistent with results from DEM simulations reported by Zhang and Evans (2019) that showed good agreement with predictions from Eq. (7) for a granular seabed.

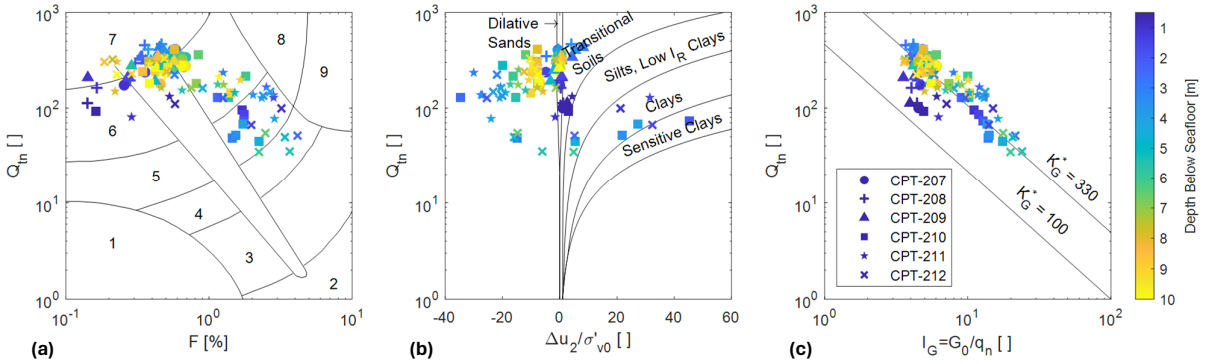

Figure 7. Soil behavioral classifications for a transect of CPT soundings at PacWave South. CPT-207 is northernmost and numbering increases in order moving south along the transect, see Fig. 2. Data points are only plotted every 0.5 m of depth for clarity.

Using appropriate values for a representative torpedo anchor ($d_{eff} = 1$ m, $L_a = 3$ m, $\rho_a = 3000$ kg/m^3, where L_a and ρ_a are anchor length and density, respectively) and a reasonable undrained strength gradient for the PWS site ($k = 8$ kPa/m for the upper 6 m) suggests an embedment depth of approximately 5 m if the anchor impacts the seabed at terminal velocity. This simple calculation implies that achieving embedment depths greater than 5 m will prove more challenging than if the profile were homogenous.

6. Conclusions

This manuscript presents an overview of an offshore testing expedition to the PacWave South Test Site off the Oregon coast. A total of 22 CPT soundings were advanced across the 2-nmi^2 site. A centroidal Voronoi tessellation approach was used to select the locations for the CPTs, based on the logic that the maximum entropy spacing was also the optimum. Interpretation of the CPT results implies that the subsurface consists of a softer, fine-grained layer over a layer of dense sand and gravel. The thickness of the soft layer decreases moving south to north through the site. While there is appreciable competent material available to provide appropriate anchor holding capacities, very simple preliminary calculations imply that achieving penetration depths that reach into the dense sand and gravel may pose a challenge.

Acknowledgements

This work was supported by the United States Department of Energy Water Power Technologies Office (Award No. DE-EE0009969), and the first author was supported by a Fulbright grant during the course of this work. This support is gratefully acknowledged. We would also like to thank Dan Hellin of PacWave and the R.T. Casey and *Seacor Lee* teams, without whom this work could not have been done.

References

Brown, C. B. 1978. "The Use of Maximum Entropy in the Characterization of Granular Media." *Proceedings of the U.S.-Japan Seminar on Continuum-Mechanical and Statistical Approaches in the Mechanics of Granular Materials*, 98–108. Sendai, Japan: Tokyo: Gakujutsu Bunken Fukyukai.

Brown, C. B. 1980. "Entropy Constructed Probabilities." *Journal of Engineering Mechanics*, 106 (EM4): 633–640.

Du, Q., V. Faber, and M. Gunzburger. 1999. "Centroidal Voronoi Tessellations: Applications and Algorithms." *SIAM Rev.*, 41 (4): 637–676. https://doi.org/10.1137/S0036144599352836.

Ehlers, C. J., A. G. Young, and J. Chen. 2004. "Technology Assessment of Deepwater Anchors." *Proceedings of the Offshore Technology Conference*, OTC-16840-MS. Houston, Texas: OTC.

Evans, T. M., and C. B. Brown. 2014. "On microstates and macrostructures for granular assemblies." *Geotechnical Special Publication*, 9.

Evans, T. M., and J. D. Frost. 2010. "Multiscale investigation of shear bands in sand: Physical and numerical experiments." *Int. J. Numer. Anal. Meth. Geomech.*, 34 (15): 1634–1650. https://doi.org/10.1002/nag.877.

Evans, T. M., and N. Zhang. 2019. "Three-Dimensional Simulations of Plate Anchor Pullout in Granular Materials." *Int. J. Geomech.*, 19 (4): 04019004. https://doi.org/10.1061/(ASCE)GM.1943-5622.0001367.

Hateley, J. C., H. Wei, and L. Chen. 2015. "Fast Methods for Computing Centroidal Voronoi Tessellations." *J Sci Comput*, 63 (1): 185–212. https://doi.org/10.1007/s10915-014-9894-1.

Hossain, M. S., C. D. O'Loughlin, and Y. Kim. 2015. "Dynamic installation and monotonic pullout of a torpedo anchor in calcareous silt." *Géotechnique*, 65 (2): 77–90. https://doi.org/10.1680/geot.13.P.153.

Jaynes, E. T. 1957a. "Information Theory and Statistical Mechanics." *Phys. Rev.*, 106 (4): 620–630. https://doi.org/10.1103/PhysRev.106.620.

Jaynes, E. T. 1957b. "Information Theory and Statistical Mechanics. II." *Phys. Rev.*, 108 (2): 171–190. https://doi.org/10.1103/PhysRev.108.171.

Jowitt, P. W. 1979. "The extreme-value type-1 distribution and the principle of maximum entropy." *Journal of Hydrology*, 42 (1–2): 23–38. https://doi.org/10.1016/0022-1694(79)90004-0.

Krieger, W. 1970. "On Entropy and Generators of Measure-Preserving Transformations." *Transactions of the American Mathematical Society*, 149: 453–464.

Lloyd, S. 1982. "Least squares quantization in PCM." *IEEE Trans. Inform. Theory*, 28 (2): 129–137. https://doi.org/10.1109/TIT.1982.1056489.

Morgenstern, M. 1963. "Maximum entropy of granular materials." *Nature*, 200 (4906): 559–560. https://doi.org/10.1038/200559b0.

O'Loughlin, C. D., M. D. Richardson, M. F. Randolph, and C. Gaudin. 2013. "Penetration of dynamically installed anchors in clay." *Géotechnique*, 63 (11): 909–919. https://doi.org/10.1680/geot.11.P.137.

Robertson, P. K. 2009. "Interpretation of cone penetration tests — a unified approach." *Can. Geotech. J.*, 46 (11): 1337–1355. https://doi.org/10.1139/T09-065.

Robertson, P. K. 2016. "Cone penetration test (CPT)-based soil behaviour type (SBT) classification system — an update." *Can. Geotech. J.*, 53 (12): 1910–1927. https://doi.org/10.1139/cgj-2016-0044.

Schneider, J. A., and R. E. S. Moss. 2011. "Linking cyclic stress and cyclic strain based methods for assessment of cyclic liquefaction triggering in sands." *Géotechnique Letters*, 1 (2): 31–36. https://doi.org/10.1680/geolett.11.00021.

Schneider, J. A., M. F. Randolph, P. W. Mayne, and N. R. Ramsey. 2008. "Analysis of factors influencing soil classification using normalized piezocone tip resistance and pore pressure parameters." *J. Geotech. Geoenviron. Eng.*, 134 (11): 1569–1586. https://doi.org/10.1061/(ASCE)1090-0241(2008)134:11(1569).

Shannon, C. E. 1948. "A Mathematical Theory of Communication." *Bell System Technical Journal*, 27 (3): 379–423. https://doi.org/10.1002/j.1538-7305.1948.tb01338.x.

Shi, B., Y. Murakami, and Z. Wu. 1998. "Orientation of aggregates of fine-grained soil: quantification and application." *Engineering Geology*, 50 (1–2): 59–70. https://doi.org/10.1016/S0013-7952(97)00082-3.

Zhang, N., and T. M. Evans. 2019. "Discrete numerical simulations of torpedo anchor installation in granular soils." *Computers and Geotechnics*, 108: 40–52. Elsevier. https://doi.org/10.1016/j.compgeo.2018.12.013.